This paper describes a mathematical model built for turbulent heat and mass transfer processes in the case of electron beam melting of titanium alloy ingots. The object of research is the conditions that ensure the quality of ingots. The model makes it possible to calculate the distribution of hydrodynamic flows in the liquid metal and temperature fields in the ingot, to determine the profile of the metal crystallization front, taking into account the interphase transition zones. The model solves the problem of finding the necessary melting regimes of ingots by calculation, in contrast to high-cost natural experiments. The thermal and hydrodynamic processes during the melting of a cylindrical ingot with a diameter of 110 mm of the newest titanium alloy Ti-6Al-7Nb for medical use were calculated and its melting parameters were determined. The small diameter of the ingot significantly facilitates its further machining. The geometry of the two-phase zone of the liquidus-solidus transition, which determines the crystallization front of the metal, was calculated. The position and geometry of this front greatly affects the quality of ingot formation and the concentration of the distribution of alloying elements and the homogeneity of the metal across its volume. A sufficiently flat crystallization front has been obtained, under which the given conditions are ensured. It was found that heat transfer in the liquid phase of the metal is mainly caused by heat and mass transfer due to its movement, and heat and mass transfer significantly depends on the power of the electron beam and its distribution on the surface of the bath. According to the calculated regimes, at the Institute of Electric Welding named after E. O. Paton, the National Academy of Sciences of Ukraine, high-quality ingots for the needs of the medical industry were smelted. The castings are used for the manufacture of light and ultra-strong endoprostheses and implants, which are chemically neutral and biologically and biomechanically compatible with the human body and do not cause rejection

Keywords: electron beam melting, titanium alloys, mathematical model, heat transfer, mass transfer, technological modes

UDC 669.187.526:51.001.57 (537.612:621.791.92)
DOI: 10.15587/1729-4061.2024.312561

CONSTRUCTION OF A MATHEMATICAL MODEL OF TURBULENT HEAT AND MASS TRANSFER PROCESSES FOR THE CASE OF ELECTRON BEAM MELTING OF TITANIUM ALLOY CASTS

Igor Krivtsun
Academician of NAS of Ukraine, Doctor of Technical Sciences, Professor, Director of the Institute*
Serhii Rymar
Doctor of Technical Sciences*
Ruslan Hubatiuk
Corresponding author
PhD*
E-mail: belichi12@gmail.com
Volodymyr Berezos
Doctor of Technical Sciences**
Dmytro Akhonin
PhD Student**
*Department of Gas Discharge Physics and Electrothermics***
Department of Metallurgy and Welding of Titanium Alloys*
***E. O. Paton Electric Welding Institute of the National Academy of Sciences of Ukraine
Kazymyr Malevych str., 11, Kyiv, Ukraine, 03150

Received date 16.07.2024
Accepted date 25.09.2024
Published date 25.10.2024

How to Cite: *Krivtsun, I., Rymar, S., Hubatiuk, R., Berezos, V., Akhonin, D. (2024). Construction of a mathematical model of turbulent heat and mass transfer processes for the case of electron beam melting of titanium alloy casts. Eastern-European Journal of Enterprise Technologies, 5 (1 (131)), 110–126. https://doi.org/10.15587/1729-4061.2024.312561*

1. Introduction

The development and introduction into production of modern effective technical solutions for smelting special titanium alloys with optimal management modes of technological smelting processes are the priority tasks of special electrometallurgy. When solving these problems, knowledge about the flow of heat and mass transfer processes in high-temperature melts during the formation of ingots is important.

Articles made of special titanium alloys are used in medicine for the manufacture of biocompatible light and strong endoprostheses and implants [1]. Such articles should have a long service life while the alloys should be alloyed with non-toxic and biologically compatible elements with the human body.

Metal implants occupy more than 60 % of the market, in which titanium and alloys based on it are the favorites. The strength indicators of titanium alloys exceed stainless steels and are at the level of cobalt alloys; such an important indicator as the modulus of elasticity of titanium alloys is two times lower than that of both of them [1]. For example, the modulus of elasticity of titanium alloys is 55...112 GPa, chrome-nickel stainless steels – 210 GPa, chrome-cobalt alloy – 240 GPa. This is a very attractive indicator of medical titanium alloys for the manufacture of osteosynthesis implants and bone and joint endoprostheses. Titanium alloys guarantee higher mechanical compatibility with bone structures of the body, in which the modulus of elasticity is approximately 27.8...30.0 GPa in the longitudinal direction, 11.0...11.5 GPa in the azimuthal and radial directions.

Copyright © 2024, Authors. This is an open access article under the Creative Commons CC BY license

Currently, the low-toxic, corrosion-resistant [2] alloy Ti-6Al-4V, which is superior to cobalt-based alloys and stainless steels in terms of biological compatibility, is widely used in medicine. In stainless steels, the mass concentration of nickel and chromium elements toxic to the human body exceeds 30 % by mass. In the Ti-6Al-4V medical alloy, the content of dangerous vanadium is an order of magnitude lower – 4 % by mass.

Designing new medical titanium alloys without the content of toxic alloying elements and their smelting technology is an urgent task of modern metallurgy.

For use in medical and surgical purposes, the newest titanium alloy Ti-6Al-7Nb has been developed, similar in mechanical properties to the alloy Ti-6Al-4V [3], in which niobium is used instead of vanadium. This alloy has excellent corrosion resistance and is harmless to the human body, with excellent biological compatibility, it is plastic and has an even lower value of the modulus of elasticity – below 40 GPa and is gradually replacing the Ti-6Al-4V alloy. The latest medical titanium alloys alloyed with niobium and zirconium and molybdenum and zirconium have also been designed.

In the future, titanium alloys may become the main metal materials for the manufacture of implants and endoprostheses, displacing stainless steel and cobalt alloys. In addition, the application of various methods of surface modification of finished articles from them – mechanical [4], thermal [5], cryogenic [6], electro-erosion [7], and chemical processing, dusting, etc., even more significantly improves such product parameters as modulus of elasticity [7], corrosion [8], and wear resistance [6, 9, 10], adhesion, biocompatibility, antibacterial properties, reduction of ion release to prevent inflammation [11].

In the Institute of electric welding named after E. O. Paton, the National Academy of Sciences of Ukraine, a technology has been devised for the production of high-quality defect-free ingots of titanium alloys, including those for medical purposes, with a guaranteed chemical composition, by the electron beam melting (EBM) technique.

One of the key processes during the smelting of high-quality ingots of titanium alloys is the crystallization of the metal. The transition of a metal from a liquid state to a solid state is accompanied by complex processes of heat and mass transfer, rapid physical and chemical processes. The non-uniformity of temperatures in the volume of the metal of the ingot affects the formation of the profile of the crystallization front and leads to differences in the structure and chemical composition of the metal in the center and periphery of the ingot, the presence of shrinkage and liquation phenomena, etc. These factors significantly affect the final metal structure of titanium alloy ingots and their quality.

In metallurgy, conducting full-scale experiments is associated with considerable material costs, which determines the prospects of using CFD modeling of high-temperature processes of heat exchange and hydrodynamics (CFD – computational fluid dynamics). Numerical modeling, based on a small amount of experimental data, and with incomparably lower material costs, makes it possible to calculate and obtain qualitative and quantitative patterns of phenomena occurring during metallurgical processes with sufficient accuracy for practice.

Numerical calculation methods and modern computer packages of mathematical modeling programs make it possible to take into account indicators of physical quantities in the form of functional dependences on the necessary parameters, for example, on temperature, pressure, etc. It is possible to set the distribution of parameter values in space and time and get significantly closer to real processes.

Naturally, the flatter the crystallization front of metal alloys and the more uniform temperature distribution in the ingot, the more uniform the distribution of alloying elements in the radial direction of the ingot. This will create conditions for obtaining a more uniform structure of the solid metal of the ingot. Given this, there is an urgent scientific task of building a mathematical model of heat and mass transfer processes during the formation of an ingot of the newest medical titanium alloy Ti-6Al-7Nb. The model should make it possible to determine by calculation such melting regimes by the EBM technique, which will provide a flatter metal crystallization front to obtain high-quality ingots. In practice, such studies, in contrast to very expensive full-scale experiments, could significantly reduce the cost of the process of searching for melting modes of ingots and increase the quality of molten metal. Similar studies for the Ti-6Al-7Nb alloy during EBM are relevant in the field of special electrometallurgy.

2. Literature review and problem statement

With the development of computer technology and the appearance on the market of powerful software packages capable of solving multiphysical problems, it became possible to implement numerical mathematical modeling of complex technical systems. This also applies to solving a number of problems of heat and mass transfer in the metallurgical industry. Sufficiently high accuracy of mathematical modeling with comparison with experimental data is confirmed by many scientific and technical publications. Thus, in [12], multiphase modeling of the metallurgical process of secondary aluminum purification with optimization of its modes was carried out. Liquid metal flows and temperature fields were calculated. The prospects and effectiveness of mathematical modeling in the search for technological modes were shown, which is confirmed by experimental data and implementation. But in the work, the side surfaces of the ingot are heated to prevent premature crystallization of the metal, which distinguishes this process from the process considered in the indicated work, in which the side surfaces of the ingot, on the contrary, are cooled. Also in the paper, the values of the main thermophysical parameters used in the calculations are given for two temperature values – liquidus and solidus. Outside of this temperature range, calculations may give some error. It can be assumed that such data on secondary aluminum were not available. In general, measuring or finding published dependences of thermophysical parameters of new alloys on temperature is a rather serious problem. In work [13], mathematical modeling of temperature fields during casting of a billet from an Al-5.25 % Cu alloy was carried out. A feature of the simulation is the meshless numerical approach used for the first time during macro-segregation simulation. In the work, the Boussinesq approximation was used to model buoyancy effects due to density differences, but the assumption was made that the density of the solid and liquid phases was constant and the same. The difference between the specified calculation model and the model proposed by the authors of this study is that it considers laminar flows of melt movement, which are characteristic of the applied technological speeds of ingot formation. For turbulent flows, this model needs refinement. The same applies to paper [14], which describes the numerical simulation of ring electromagnetic mixing in the process of uniform casting with direct cooling of aluminum alloy blanks. The simulation made it possible to investigate flow regimes,

isotherms, and the metal solidification profile. Comparison of simulation results and experiments showed that the model provides good agreement with real processes. The results of numerical mathematical modeling [15] of vertical casting of aluminum alloys show that the temperature distribution and the velocity field in the melt and in the two-phase region differ significantly under the conditions of different schemes for supplying liquid metal. The calculations give a clear idea of the distribution of liquid metal flows and temperature changes in the cross sections of the ingot. A comparison with experimental data shows that mathematical models are a powerful tool for optimizing heat and mass transfer processes in liquid metal ingots. The numerical method of finite differences was used in the problem considered in the work, but for the problem of the authors of this study, the numerical method of finite elements will be a more acceptable method. In work [16], numerical mathematical modeling provided predictions on the limit speed of casting. It was established that in case of intensive supply of molten metal into the bath, turbulent flows in the melt occur, which is facilitated by the developed forced convective flows downstream. The paper uses the averaged values of the main thermophysical parameters, as in [12], except for thermal conductivity. Averaging the values introduces a certain error in the obtained calculation results in comparison with reality. It can also be assumed here that this problem of increasing the accuracy of calculations has not been solved due to the lack of dependence of these data on temperature. The results of calculations of mathematical modeling of casting aluminum ingots [17] show that in this process the temperature field, flows of liquid metal and the profile of the crystallization boundary strongly depend on the intensity of ingot cooling. This, in turn, affects the macro- and microstructure of the metal, which determine the quality of the resulting ingots. The model made it possible to obtain a good match of the results with reality, which was carefully confirmed by laboratory test data. However, the work does not include the equations of the mathematical model and the boundary conditions that were used for calculations, which makes its analysis impossible. The same applies to work [18], which shows the importance of modeling a complex of metallurgical processes during the smelting of large-sized steel ingots. It was concluded that mathematical modeling began to play an extremely important role in the search for melting modes, which significantly reduced the cost of their search and increased the quality of the obtained metal. The analysis of heat transfer in the crucible during electron beam melting of steel [19] revealed that in order to better understand the thermal behavior of the metal in the crucible, it is advisable to use numerical three-dimensional modeling of these processes. The comparison of measured and calculated temperatures showed a satisfactory agreement of the results, which proves that the numerical model is an effective tool for modeling industrial processes. But in the work, experimental confirmation of the model was obtained when the source of heating of the electron beam on the surface of the melt is simulated by the thermal effect of the arc. This leads to some inconsistency of the conducted experiment, both with mathematical modeling and with the process of heating by an electron beam. In works [20, 21], the heat capacity of the phase transition is calculated using the Gaussian function, which is multiplied by the value of the latent heat of fusion of the metal. But this requires an additional determination of the width of the span of this function along the abscissa axis, which may affect the accuracy of the obtained data. In works [22, 23], the problem of mathematical modeling of heat and mass transfer in the case of forming ingots of titanium alloy Ti-6Al-4V with a diameter of 400 and 600 mm was solved. The surface of the melt in the crystallizer is heated by two electron guns. The laminar [23] and turbulent [22] motion of the metal melt in the crystallizer was considered. However, approximations of the thermophysical parameters of the alloy from the temperature at the points of phase transitions of the metal have sharp stepwise jumps in the values of the functions. This can lead to errors in the numerical solution of differential equations using the finite element method for the temperature values at these points. Also, the parameters of heat dissipation into the wall of the crystallizer from the liquid metal of the bath and the parameters of heat radiation from the ingot surfaces are also quite roughly defined.

Thus, our review of the literature demonstrates the possibility of fairly high accuracy of numerical mathematical modeling of metallurgical processes during the melting of ingots and a significant reduction in the cost of searching for the parameters of melting modes, which significantly increased the quality of the molten metal. However, some issues are not resolved in the considered works, in particular, they do not take into account the dependence of the thermophysical parameters of the metal on the change in temperature [12, 16], and where it is taken into account, there are sharp jumps and breaks in the values of these functions at the points of phase transitions [22, 23]. Not turbulent, but laminar flows of liquid metal were considered [13, 14, 23]. Basic equations of mathematical models are not given [17, 18]. The heat capacity of the phase transition is not calculated rationally enough [20, 21]. The parameters of heat removal into the wall of the crystallizer need clarification [22, 23]. All works consider alloys different from the one used in this work. In most cases, metal melts are defined as incompressible rather than incompressible liquids. Shapes of crystallizers and their sizes also differ. This also applies to the geometry of the jets of liquid metal poured into the crystallizers. Solving these issues could increase the accuracy of calculations in the case of a through-flow crystallizer of small diameter with a relatively high rate of liquid metal pouring into it, sufficient to ensure the turbulence of melt flows in the crystallizer.

3. The aim and objectives of the study

The purpose of our work is to determine patterns in the turbulent processes of heat and mass transfer in the case of electron beam melting of ingots of titanium alloys based on the construction of a mathematical model of these processes. The practical use of this model makes it possible to determine the parameters of technological melting regimes, which ensure high quality ingots of titanium alloy Ti-6Al-7Nb for medical purposes, based on the calculated shape of the metal crystallization front profile.

To achieve the goal, the following tasks were set:

– to build a mathematical model of thermal processes in the ingot under the condition of the turbulent nature of the movement of the molten metal;

– to construct a mathematical model of turbulent hydrodynamic processes in the ingot;

– to take into account the thermophysical characteristics of the metal, including their change in the interphase transition zones;

– to establish by using mathematical modeling methods the distribution of turbulent hydrodynamic flows and temperature fields in the ingot and metal crystallization front.

4. The study materials and methods

The object of our study is the conditions that ensure the quality of ingots of the newest titanium alloy Ti-6Al-7Nb for medical use when smelted by the electron beam melting technique. The subject of the study is the regularities of the distribution of hydrodynamic flows in liquid metal and temperature fields in the ingot, which affect the crystallization front of the metal, which is an important factor in obtaining high-quality ingotsThe main hypothesis of the research assumes that the position of the electron beam on the surface of the mirror of the bath of molten metal and its power are the main factors influencing the process of the formation of the crystallization front of the metal in the ingot. Accordingly, the quality of the metal in the ingot depends on this.

Research was carried out for an ingot with a diameter of 110 mm with a speed of its extraction in a continuous crystallizer of 20 kg/h. This speed of ingot formation and intensive supply of liquid metal to the crystallizer contributes to the fact that the flows in the bath have a turbulent nature of movement in most of its parts:

– the standard (classical) k-ε model of turbulence is applied, which is based on the fact that the Reynolds numbers are large, the turbulence is in equilibrium in the wall regions, and the energy is equal to the dissipation. This somewhat limits the accuracy of the model, especially near the walls, but is a trade-off with significant savings in computing resources;

– the method with a fixed grid is applied. In this method, the liquid and solid phases are treated as a single liquid-phase region, and the solid metal is simulated as a volume in which the metal motion is completely suppressed by the Darcy braking force (except for the ingot withdrawal rate);

– the interphase boundary "liquidus-solidus" of the L-S alloy is expressed by a viscous transition zone. The liquid phase is defined by a temperature that exceeds the liquidus temperature, the solid phase is defined by a temperature that is below the solidus temperature. The transition zone is limited by these temperatures, in which the parameters of the metal change according to a given law relative to the volume fraction of a certain phase;

– the volume fraction of the metal in the transition zone, depending on the temperature, is described by a smoothed function using the mathematical error function "erf";

– approximation dependences of thermophysical parameters of titanium alloy are constructed in such a way that they have smooth transitions with stepwise jumps of values in phase transitions using the "erf" function. For this purpose, the temperature limits of phase transitions are somewhat artificially expanded [24];

– the considered turbulent dynamic viscosity coefficient μ_T is not a property of the liquid but is determined by the nature of the flow according to the Boussinesq hypothesis;

– coefficient of turbulent thermal conductivity λ_T in liquid metal is used, which takes into account heat transfer from turbulent pulsations of metal flows;

– the classic Kays-Crawford model is used, which provides approximate values of Prandtl turbulent numbers Pr_T with overestimation of Nusselt numbers Nu, but is suitable for approximate calculations and forecasts;

– it is believed that the distribution of thermal power from the center of the electron beam on the surface of the bath mirror varies according to the Gaussian law.

Adopted simplifications are as follows:

– it is considered that the metal melt during the melting of the ingot is poured into the crystallizer continuously at a constant speed and with the maintenance of the average speed of drawing the ingot for the entire time of melting;

– a liquid metal bathtub mirror is considered a flat surface;

– the lower part of the calculation area is limited by the plane of the cross-section of the lower part of the ingot at such a distance from its upper part where thermal processes no longer affect the thermal processes in its upper part in the region of the metal crystallization front;

– molten metal is considered an incompressible viscous liquid;

– since the pressure change in the molten metal is insignificant, the specific heat capacity from the work performed as a result of the pressure change can be neglected;

– it is considered that the thermal conductivity of the copper wall of the crystallizer is ideal;

– to take into account the flow near the walls, analytical wall functions are used, which make theoretical deviations from the physical wall but give acceptable forecasts;

– the heat capacity in the α-β and L-S phase transition zones of the titanium alloy is taken into account by adding the equivalent heat capacity and the heat capacity, which takes into account the latent heat of phase transitions;

– heat capacity, which takes into account the latent heat of vaporization of the metal, is indirectly taken into account by the specific power of evaporation from the surface.

The mathematical model was built on the basis of fundamental physical laws of heat transfer, hydrodynamic laws of heat and mass transfer. Time-averaged equations such as the Reynolds-averaged Navier-Stokes (RANS) equations, the Boussinesq approximation and his hypothesis for turbulent flow, and the Darcy braking force were applied. The basis of the calculations was the standard k-ε model of turbulence. The finite element numerical method and an HP ProLiant ML350 Gen9 SFF server with two 14-core Xeon E5-2680V4/2.4 GHz processors were used to calculate the three-dimensional mathematical model. Smelting of ingots took place on the research equipment at the Institute of Electric Welding named after E. O. Paton, the National Academy of Sciences of Ukraine.

The necessary regimes and parameters of melting of the ingot were searched by the method of mathematical modeling of the thermal and hydrodynamic processes occurring in it.

5. Results of investigating a three-dimensional mathematical model for calculating turbulent processes of heat and mass transfer

5. 1. Mathematical model of thermal processes in a cylindrical ingot under the condition of turbulent movement of the metal melt

For a stationary process under the condition of turbulent movement of liquid metal, taking into account the phase transition from its liquid to solid state, the heat transfer equation, W/m^3, can be written in the following form [22, 25]:

$$\rho C_p \mathbf{u}\cdot\nabla T+\nabla\cdot\mathbf{q}=Q+Q_p+Q_{vd}; \quad (1)$$

$$\mathbf{q}=-\lambda_{eff}\nabla T. \quad (2)$$

Here, ρ is the specific density of the metal, kg/m^3; C_p is the specific heat capacity of the metal, which takes into account the heat of the phase transition, J/(kg·K); $\mathbf{u}$ is the metal movement speed vector determined by hydrodynamic calculation, m/s; ∇ – nabla operator, m^{-1}; T – temperature, K;

q – specific heat flow vector due to thermal conductivity (heat flow density), W/m^2; Q – specific power from additional internal heat sources (in the problem under consideration, such sources are absent and Q=0 W/m^3); Q_p is the specific heat capacity from the work performed when the pressure changes (since the pressure change is insignificant, this heat capacity can be neglected, i.e. $Q_p \approx 0$ W/m^3); Q_{xd} is viscous dissipation [26], or thermal power per unit volume, W/m^3=Pa/s, released as a result of performing work with the presence of viscous friction with the presence of turbulence in the metal melt and determines the intensity of irreversible transformation mechanical energy for heat (in the problem under consideration, the value of Q_{xd} is not significant since the speed of movement of the metal to release heat is not high, so this parameter can be ignored in the heat problem, $Q_{xd} \approx 0$ W/m^3); λ_{eff} is the effective coefficient of thermal conductivity, which takes into account molecular and turbulent thermal conductivity, W/(m·K). Hereafter, to simplify the writing of the equations, the dependence of the thermophysical parameters of the metal (T), $\lambda_{eff}(T)$, $C_p(T)$ etc. on temperature is not explicitly shown.

To determine the specific heat capacity of the metal C_p, taking into account the latent heat of fusion – enthalpy $H_{L\text{-}S}$, J/kg, in the phase transition, the Apparent Heat Capacity Method [27] is used. In the method, it is considered that the release of latent heat of fusion during the crystallization of the metal occurs in the temperature range between the temperature of the liquidus T_L and the temperature of the solidus T_S. Here, the indices L and S denote liquidus and solidus, that is, liquid and solid phases. In this temperature range, the specific heat capacity C_p:

$$C_p = C_{eq} + C_{L\text{-}S}, \tag{3}$$

where C_{eq} is the equivalent heat capacity of the transition zone; $C_{L\text{-}S}$ is the heat capacity of the latent heat of the phase transition.

The equivalent heat capacity is determined from the following formula:

$$C_{eq} = \frac{F_{L-S}\rho_L C_L + (1-F_{L-S})\rho_S C_S}{F_{L-S}\rho_L + (1-F_{L-S})\rho_S}. \tag{4}$$

Here, $F_{L\text{-}S}$ is an approximation function that determines the distribution of the volumes of liquid and solid metal in the two-phase liquidus-solidus zone in the temperature range $T_L...T_S$ and will be defined below; ρ_L, ρ_S and C_L, C_S are, respectively, the specific density of the metal and its heat capacity at the liquidus and solidus temperature points.

To determine the heat capacity $C_{L\text{-}S}$, an approximation dependence is used that meets the following condition [12, 28]:

$$\int_{T_S}^{T_L} C_{L-S}(T)\,\mathrm{d}T = H_{L-S}. \tag{5}$$

The nature of the heat capacity $C_{L\text{-}S}$ distribution in the transition zone corresponds to the temperature derivative of the approximation function $F_{L\text{-}S}$. This derivative will also be defined below.

Accounting for the latent heat α–β of the $H_{\alpha-\beta}$ transition is similar, but for its temperature range $T_\alpha...T_\beta$ with its approximation function $F_{\alpha-\beta}$, which determines the distribution of phase volumes in the artificial temperature range $T_\alpha...T_\beta$ of the α–β phase transition zone and also will be determined below, and by the heat capacity of the latent heat of the phase transition $C_{\alpha-\beta}$.

The effective coefficient of thermal conductivity is calculated according to the following formula:

$$\lambda_{eff} = \lambda + \lambda_T, \tag{6}$$

where λ is the coefficient of molecular thermal conductivity, W/(m·K); λ_T is the coefficient of turbulent thermal conductivity in liquid metal, W/(m·K), taking into account the additional heat transfer mechanism associated with turbulent pulsations of metal flows. The values of λ_T can be obtained from the following formula [29]:

$$\lambda_T = \frac{C_p \mu_T}{\mathrm{Pr}_T}. \tag{7}$$

Here, μ_T is the coefficient of turbulent dynamic viscosity, Pa·s, the definition of which will be discussed below; Pr_T is the turbulent Prandtl number, which can be calculated with sufficiently high accuracy for gases and liquids in the case of $\mathrm{Pr}_T \le 1$ and $\mathrm{Pr} \ge 1$ [30] by an approximation formula in accordance with the Kays and Crawford model [31, 32]:

$$\mathrm{Pr}_T = \left\{ \begin{array}{l} \dfrac{1}{2\mathrm{Pr}_{T\infty}} + \dfrac{0.3}{\sqrt{\mathrm{Pr}_{T\infty}}} \cdot \dfrac{C_p\mu_T}{\lambda} - \left(0.3\dfrac{C_p\mu_T}{\lambda}\right)^2 \times \\ \times \left[1 - \exp\left(-\dfrac{\lambda}{0.3 C_p \mu_T \sqrt{\mathrm{Pr}_{T\infty}}}\right)\right] \end{array} \right\}^{-1}, \tag{8}$$

where $\mathrm{Pr}_{T\infty}$ is the turbulent Prandtl number at a long distance from the wall, taken equal to 0.85, with $\mathrm{Pr}_T < 1.7$, and in the case of $\mathrm{Pr} \to 0$, heat transfer will take into account only molecular conduction. In general, the Prandtl number takes into account the influence of the physical properties of the coolant on heat transfer.

For liquid metal flows at $\mathrm{Pr}_T \gg 1$ and $\mathrm{Pr} \ll 1$ [30], the Kays-Crawford model holds but gives overestimated predictions of the Nusselt numbers Nu. For liquid metals, $\mathrm{Pr} \le 1$, and does not strongly depend on temperature. Therefore, formula (8) for liquid metals can be used for estimation calculations in the first approximation.

The formula for determining the Pr_T number is known, obtained in [33], on the basis of data [34], based on simulated transport equations for turbulent kinetic energy and turbulent heat flow. The peculiarity of the formula is that it gives average values of Pr_T throughout the boundary layer, as it does not take into account their spatial distribution. In the case of flow in pipes and channels:

$$\mathrm{Pr}_T = 0.9 + \frac{182.4}{\mathrm{Pr}\cdot \mathrm{Re}^{0.888}}. \tag{9}$$

Based on equation (9), in [30], an expression for calculating the Prandtl number at a large distance from the wall was introduced into the Kays-Crawford model (8) for more accurate prediction of heat transfer in fluids with a low Prandtl number:

$$\mathrm{Pr}_{T\infty} = 0.85 + \frac{D}{\mathrm{Pr}\cdot \mathrm{Re}^{0.888}}. \tag{10}$$

Here D is a constant equal to 100 (but it can be refined); Re is the Reynolds number.

Formula (10) makes it possible to use expression (8) for all molecular Prandtl numbers for the conditions of a fully developed flow, as well as for a thermal flow developing under various boundary conditions at the wall [30]. This gives refined Pr_T values for low Prandtl number flows (liquid metals). The refined model (8), (10) was named the extended Kays-Crawford model. For liquids and gases, the model reduces to the original Kays-Crawford model.

With regard to the flows of liquid metal in the bath considered in this paper, it should be noted that in this case both Kays-Crawford models will give an approximate result. The classical model gives exaggerated values of Nu numbers for liquid metals, and the extended model requires the determination of Reynolds numbers, which depend on the characteristic geometric size of the system and the flow rate. For pipes and channels, Reynolds numbers are determined uniquely. But their definition in the researched problem is a significant challenge. Their imprecise definition can give a higher error than in the case of using the classic Kays-Crawford model. In addition, the extended model was developed based on data obtained in the case of flows in pipes and channels.

Also, for estimation calculations of the value of the coefficient of turbulent thermal conductivity λ_T, in formula (7) it is possible to directly specify values of Pr_T from the range of their predicted values. For example, in work [22], data on the values of Pr_T numbers, which lie in the range of 1...10 for liquid metal, were given.

The classic Kays-Crawford model was used, which gives an approximate value of Pr_T. The calculated parameters of the considered processes are compared with the results obtained at the given Pr_T numbers using formula (7). They were comparable in terms of Pr_T numbers in area 1, where the depth of the bath and the flow of molten metal are close. Comparisons were also made with the results obtained using the extended Kays-Crawford model with a change in Reynolds numbers in the range $Re=10^4...10^5$. Changes in the values of Re numbers affected the flow of molten metal in the bath, but the depth of the bath did not change significantly.

In the transition zone, the coefficient of turbulent thermal conductivity was not used. The effective thermal conductivity in this zone was calculated from the molecular thermal conductivities of the liquid and solid phases according to the following formula:

$$\lambda_{eff}=F_{L\text{-}S}\lambda_L+(1-F_{L\text{-}S})\lambda_S. \quad (11)$$

To take into account heat transfer, a near-wall function is used, which is based on the universal temperature distribution near the wall. At the same time, the heat flow through the wall q_w, W/m^2, from the Launder-Spalding model, will be equal to [35, 36]:

$$-\mathbf{n}\cdot\mathbf{q}=q_w=\rho C_p u_\tau \frac{T_w-T}{T^+}. \quad (12)$$

Here $\mathbf{n}$ is the vector normal to the surface; u_τ is the friction speed given by the properties of the wall, m/s; T_w – wall temperature, K; T^+ is a dimensionless value of temperature, which is calculated according to the empirical formula [29, 37] with dimensionless coefficients δ_w^+, δ_{w1}^+, δ_{w2}^+ and β:

$$T^+=\begin{cases}\Pr\delta_w^+,\ \delta_w^+<\delta_{w1}^+;\\ 15\Pr^{2/3}-\dfrac{500}{\delta_w^{+2}},\ \delta_{w1}^+\le\delta_w^+<\delta_{w2}^+;\\ \dfrac{\Pr_T}{\kappa}\ln\delta_w^+ +\beta,\ \delta_{w2}^+\le\delta_w^+;\end{cases} \quad (13)$$

$$\delta_w^+=\frac{\delta_w\rho\sqrt{C_\mu^{1/2}k}}{\mu};\ \delta_{w1}^+=\frac{10}{\Pr^{1/3}};\ \delta_{w2}^+=10\sqrt{10\frac{\kappa}{\Pr_T}};$$

$$\Pr=\frac{C_p\mu}{\lambda};\ \beta=15\Pr^{2/3}-\frac{\Pr_T}{2\kappa}\left[1+\ln\left(1000\frac{\kappa}{\Pr_T}\right)\right];$$

κ is Von Karman's constant, equal to 0.41.

Formula (12) is oriented to sufficiently large Reynolds numbers, and for their small values, the formula gives an approximate result.

Equations (7), (8), (12), and (13) combine thermal and hydrodynamic problems in the statement of non isothermal flow.

Heat supply in the model is balanced by heat removal due to evaporation and radiation from the mirror of the metal bath; heat transfer to the crystallizer; radiation from the surface of the ingot into the crystallizer below the point of detachment of the ingot from the walls of the crystallizer; radiation outside the crystallizer; thermal conductivity of the ingot at the lower limit of the calculation area.

Below are the boundary conditions for heat fluxes.

Fig. 1 schematically shows 1/2 part of the ingot in its conventional cross-section along its vertical axis of symmetry in the middle of the conditional spot on the surface of the bath from the stream of liquid metal pouring into the bath. That is, 1/2 part of the model is considered, since its conditional parts are symmetrical and identical in this cross-section.

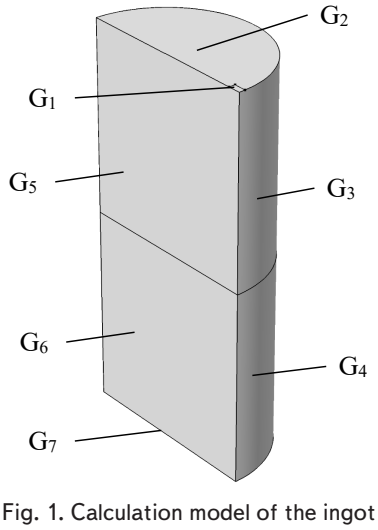

Fig. 1. Calculation model of the ingot

At the boundary G_1, which is limited by the area of pouring liquid metal into the crystallizer, there is an entrance to the system – Inflow, and the following equations correspond to it [25]:

$$-\mathbf{n}\cdot\mathbf{q}=\rho\Delta H\mathbf{u}\cdot\mathbf{n}; \quad (14)$$

$$\Delta H=\Delta H_T+\Delta H_p; \quad (15)$$

$$\Delta H_T=\int_{T_{in}}^{T}C_p\mathrm{d}T. \quad (16)$$

Here, ΔH is the change in melt enthalpy (thermal energy), which depends on the temperature difference and pressure difference [38] (Maxwell's ratio), respectively, on the components ΔH_T and ΔH_p, J/kg; **u** is the speed of the melt jet at the inlet; T_{in} is the temperature of the metal at the inlet (the temperature of the metal poured from the intermediate container [39]), K.

As was noted in the description before using equation (1), if the change in pressure can be neglected, then the ΔH_p component can also be omitted here. In this case, an isobaric process with p=const is considered, and equation (15) will take the form $\Delta H=\Delta H_T$, where the change in enthalpy ΔH_T is determined by Kirchhoff's thermochemical law (16) [40, 41]. Therefore, the boundary G_1 will correspond to the condition of the 2nd kind for an "open" wall. For estimation calculations, this limit can also be determined by the condition of the isothermal process of the 1st kind, setting instead of formulas (14) to (16) the temperature on the surface of the region $T=T_{in}$.

At the boundary G_2, which is limited by the area of the mirror of the metal melt in the crystallizer, with the exception of the boundary G_1, there is heating of the melt from the electron beam (condition of the 2nd kind), its cooling due to evaporation (condition of the 2nd kind), and radiation (condition of the 3rd kind):

$$-\mathbf{n}\cdot\mathbf{q}=q_{eb}-q_{ev}-q_{rad2}. \quad (17)$$

Here q_{eb} is the specific heat flux averaged over the surface of the molten metal bath mirror from the electron beam that uniformly heats this surface, W/m^2:

$$q_{eb}=P_{eb}/S_{dz}; \quad (18)$$

P_{eb} – thermal power from the electron beam, W; S_{dz} – surface area of the molten metal bath mirror, m^2; $S_{dz}=\pi r^2$; r is the radius of the molten metal bath mirror, m. The heat flux q_{eb} is distributed over the surface of the molten metal bath mirror, usually uniformly (14) or (and) according to the Gaussian distribution along the radius. In the latter case, the Gaussian distribution of thermal power from the electron beam on the surface of the bath and the radius of the spot from the beam are taken into account; q_{ev} – specific heat flux due to evaporation of liquid metal from the surface of the bath mirror, W/m^2; q_{rad2} is the specific heat flux of radiation from the surface of the liquid metal bath mirror, W/m^2, [42]:

$$q_{rad\,2}=\varepsilon_2\sigma\left(T_{vault}^4-T^4\right); \quad (19)$$

ε_2 is the dimensionless coefficient of the reduced degree of blackness of the system of surfaces of the bodies "liquid metal of the bath mirror – the vault of the vacuum chamber", between which the process of radiant heat exchange takes place; $\sigma=5.67\cdot10^{-8}$ W/(m$^2\cdot$K^4) – Stefan-Boltzmann constant; T_{vault} is the temperature of the vacuum chamber vault above the bathtub mirror.

The coefficient of the reduced degree of blackness of the system of surfaces of two bodies a and b on the i-th boundary is calculated according to the following formula [43]:

$$\varepsilon_i=\frac{1}{1/\varepsilon_a+1/\varepsilon_b-1}. \quad (20)$$

Here, ε_a and ε_b are coefficients of the degree of blackness of the respective surfaces.

At the boundary G_3, which is limited by the walls of the crystallizer, there is both convective and radiant heat exchange (conditions of the 3rd kind):

$$\begin{cases}-\mathbf{n}\cdot\mathbf{q}=-q_{conv3}, T_{in}\geq T>T_L;\\ -\mathbf{n}\cdot\mathbf{q}=-q_{conv3'}-q_{rad3'}, T_L\geq T\geq T_{sep};\\ -\mathbf{n}\cdot\mathbf{q}=\ q_{rad3}, T<T_{sep},\end{cases} \quad (21)$$

where q_{conv3} is the specific heat flow in the case of convective heat exchange, W/m^2, passing along the height through the section of the crystallizer wall with temperature T_{cryst}, which is in contact with liquid metal having a temperature higher than the liquidus temperature T_L [42]:

$$q_{conv3}=h_3(T_{cryst}-T); \quad (22)$$

h_3 is the coefficient of heat transfer from the surface of the liquid metal of the ingot, which integrally takes into account the heat transfer from it through the wall of the crystallizer to the cooling water, W/(m$^2\cdot$K). In this section, it is taken as such that it decreases linearly from the value of h_{in} to the value of h_L as the temperature of the melt decreases:

$$h_3=h_L+\left(h_{in}-h_L\right)\frac{T-T_L}{T_{in}-T_L}; \quad (23)$$

q'_{conv3} is the specific heat flow in the case of convective heat exchange, W/m^2, passing in height through the section of the crystallizer wall that is in contact with the metal of the ingot, which has a temperature below the liquidus temperature T_L and higher than the temperature of the detachment of the ingot from the wall of the crystallizer T_{sep} due to shrinkage metal because of its cooling:

$$q'_{conv3}=h'_3\left(T_{crost}-T\right); \quad (24)$$

h'_3 is the coefficient of heat transfer from the surface of the ingot metal, which integrally takes into account the heat transfer from it through the wall of the crystallizer to the cooling water, W/(m$^2\cdot$K). In this section, it is taken so that with a decrease in the temperature of the ingot metal, it decreases according to the law of the approximation function F_{L-sep} (to be defined below), from the value of h_L to the value of h_{sep}:

$$h'_3=h_L F_{L\ sep}+h_{sep}\left(1\quad F_{L\ sep}\right); \quad (25)$$

q'_{rad3} is the specific heat flux from radiation from the surface of the ingot metal, W/m^2, falling on the area of the crystallizer wall with the temperature of the ingot metal below the liquidus temperature T_L and above the ingot separation temperature from the crystallizer wall T_{sep}:

$$q'_{rad3}=\varepsilon'_3\sigma\left(T_{cryst}^4-T^4\right); \quad (26)$$

ε'_3 – dimesionless coefficient of the reduced degree of blackness of the system of body surfaces in this area:

$$\varepsilon'_3=\varepsilon_3\left(1-F_{L\ sep}\right); \quad (27)$$

ε_3 is the dimensionless coefficient of the reduced degree of blackness of the system of surfaces of bodies "cast metal – wall of the crystallizer", between which the process of radiant heat exchange takes place; q_{rad3} is the specific heat flux from

radiation from the surface of the ingot metal, W/m^2, falling on the area of the crystallizer wall with the temperature of the ingot metal below the ingot separation temperature from the crystallizer wall T_{sep}:

$$q_{rad3} = \varepsilon_3 \sigma \left(T_{cryst}^4 - T^4 \right). \quad (28)$$

At the boundary G_4, which is limited by the vertical walls of the ingot that came out of the crystallizer, there is only radiative heat exchange (condition of the 3rd kind):

$$-\mathbf{n} \cdot \mathbf{q} = q_{rad4}. \quad (29)$$

q_{rad4} is the specific heat flux of radiation from the side surface of the ingot metal, W/m^2, falling on the wall of the vacuum chamber with the temperature T_{wall}:

$$q_{rad4} = \varepsilon_4 \sigma \left(T_{wall}^4 - T^4 \right). \quad (30)$$

ε_4 is the dimensionless coefficient of the degree of blackness of the system of surfaces of bodies "cast metal – wall of the vacuum chamber" in this area.

On the boundaries G_5 and G_6, which are limited by the cross-sectional plane – Symmetry, which runs along the vertical axis of symmetry of the ingot along its height and in the middle of a conditional spot on the surface of the bath from a jet of liquid metal pouring into the bath (condition of the 2nd kind):

$$-\mathbf{n} \cdot \mathbf{q} = 0. \quad (31)$$

The boundary G_7 is limited by the cross-sectional plane of the lower part of the ingot at such a distance from its upper part, where thermal processes no longer affect the thermal processes in its upper part in the region of the metal crystallization front. This border is a conditional exit from the system – Outflou. The distance to it is determined by iterative calculation. On this boundary, the condition of the 2nd kind of adiabatic process of the "closed" wall (thermal insulation) is selected:

$$-\mathbf{n} \cdot \mathbf{q} = 0. \quad (32)$$

This boundary G_7 can also be described by the equations of the 2nd kind condition (14) to (16), for **u** is the casting speed, and the approximate value of the temperature T_7 on the boundary G_7 is chosen as the temperature value of the lower boundary of the integral of equation (16), which is specified when making calculations.

Naturally, both the one and the second condition at the boundary G_7 will give only approximate calculated values of the temperatures in the lower part of the ingot.

The vault and walls of the vacuum chamber have water cooling.

5. 2. Mathematical model of turbulent hydrodynamic processes in the melt of a cylindrical ingot

Mathematical modeling of hydrodynamic processes in the case of continuous supply of incompressible titanium melt to the crystallizer is performed using the model of Reynolds-averaged Navier-Stokes (RANS) equations for momentum conservation and the continuity equation for mass conservation. For a stationary process, the model takes the following form [22, 36, 44, 45]:

$$\rho(\mathbf{u} \cdot \nabla)\mathbf{u} = \nabla \cdot (p\mathbf{I} + \mathbf{K}) + \mathbf{F}_d + \rho\mathbf{g}; \quad (33)$$

$$\mathbf{K} = (\mu + \mu_T)[\nabla \cdot \mathbf{u} + (\nabla \cdot \mathbf{u})^T]; \quad (34)$$

$$\rho \nabla \cdot \mathbf{u} = 0, \quad (35)$$

where p is the average pressure value, Pa; **I** is a unit tensor; **K** – tensor of viscous stresses, Pa; $\mathbf{F}_d$ is the Darcy braking force vector, which is introduced artificially to reduce and suppress velocities in the viscous and solid zones, Pa/m; **g** – free fall acceleration vector, m/s^2; μ is the coefficient of molecular viscosity of the liquid metal, Pa·s.

The introduction of the coefficient of turbulent dynamic viscosity μ_T into the Navier-Stokes equation, which is not a property of the liquid, but is determined by the nature of the flow, is determined by the Boussinesq hypothesis for turbulent flow, by analogy with Stokes' law for laminar flow. Since in equation (33) in the last term ρ depends on the temperature T, the idea of the Boussinesq approximation is used in this case. In it, the product ρ**g** affects the process of convection due to changes in temperature, due to the fact that the acceleration of free fall g is of sufficient magnitude for this product to be significant.

Averaging according to Reynolds leads to the non-closure of the Navier-Stokes equations, which can be closed by semi-empirical turbulence models, which determine the value of the coefficient of turbulent dynamic viscosity μ_T. For the numerical calculation of hydrodynamic problems, there are several models that differ from each other in the accuracy of the description of the turbulent flow and the complexity of the solution. One of the most widely used models is the k-ε model of turbulence [36, 44, 45], the standard version of which was devised and improved in works [35, 46–48]. The model has a fairly high rate of convergence of results and uses relatively small volumes of the computer's operational memory. More complex and accurate turbulence models make it possible to more accurately calculate the structure of motion in near-wall regions. But in the problem under consideration, this is not so important since in these areas there is mostly solid metal, the direction and speed of which is known, and is determined by the speed of drawing the ingot.

The standard k-ε model is one of the most common models of turbulence – Turbulent Flow. Two additional transport equations and two dependent variables are introduced into the model: k – turbulent kinetic energy (kinetic energy of turbulent pulsations), J/kg; ε is the rate of turbulent dissipation (the rate of energy dissipation of turbulent pulsations), J/(kg·s)=m^2/s^3. The k-ε turbulence model relies on several assumptions, the most important of which is that the Reynolds number is sufficiently large. It is also important that the turbulence is in equilibrium in the near-wall regions. This means that energy equals dissipation. These assumptions limit the accuracy of the model as they do not always correlate with reality. Thus, the model does not always respond properly to flows with pressure gradients, which can lead to an underprediction of the spatial extent of recirculation zones. In the case of simulation of rotating flows, the model may show incomplete agreement with the experiment. The model is suitable for incompressible flows, weakly compressible flows, and compressible flows with low Mach numbers (less than 0.3). But in most cases, the limited accuracy of the model is a fair trade-off for the volume of computational resources saved, compared to using more complex turbulence models.

Turbulent dynamic viscosity, Pa·s, in the k-ε turbulence model:

$$\mu_T = \rho C_\mu \frac{k^2}{\varepsilon}. \quad (36)$$

Here, C_μ=0.09 is Taudsen's empirical constant [49].

The values of k and ε are determined by solving two equations [29, 36]. The differential equation (with the dimensionality of terms in Pa/s) in the partial derivatives of the first order for the kinetic energy of turbulent pulsations k:

$$\rho(\mathbf{u}\cdot\nabla)k = \nabla\cdot\left[\left(\mu+\frac{\mu_T}{\sigma_k}\right)\nabla k\right]+\mu_T P(\mathbf{u})-\rho\varepsilon, \quad (37)$$

where σ_k=1 is a constant; $P(\mathbf{u})$ is a function that takes into account the occurrence (production) of turbulence $P(\mathbf{u})$, Pa/s:

$$P(\mathbf{u}) = \nabla\cdot\mathbf{u}:\left(\nabla\cdot\mathbf{u}+(\nabla\cdot\mathbf{u})^T\right). \quad (38)$$

The differential equation (with the dimensionally of terms Pa/s^2) in the partial derivatives of the first order for the energy dissipation rate of turbulent pulsations ε:

$$\rho(\mathbf{u}\cdot\nabla)\varepsilon = \nabla\cdot\left[\left(\mu+\frac{\mu_T}{\sigma_\varepsilon}\right)\nabla\varepsilon\right]+$$
$$+C_{\varepsilon1}\frac{\varepsilon}{k}\mu_T P(\mathbf{u})-C_{\varepsilon2}\rho\frac{\varepsilon^2}{k}. \quad (39)$$

Here the constants σ_ε=1.3; $C_{\varepsilon1}$=1.44; $C_{\varepsilon2}$=1.92, the values of which for this problem can be taken from the Launder-Sharma [46, 50] and Launder-Spalding [35] models.

The Darcy braking force, Pa/m, can be calculated from the following formula [51–53]:

$$\mathbf{F}_d = \frac{C(1-F_{L-S})^2}{q+F_{L-S}^3}(\mathbf{u}-\mathbf{u}_{cast}), \quad (40)$$

where $C\approx10^2...10^4$ kg/(m^{3}s); $q\approx10-2...10^{-4}$ are constants whose ratio C/q must be sufficient to suppress movement in solid metal when $F_{L\text{-}S}$=0 (except for the melting rate of the ingot $\mathbf{u}_{cast}$). In a liquid metal, when $F_{L\text{-}S}$=1, the Darcy force $\mathbf{F}_d$=0, and should not affect the motion [51]. In the transition zone, the current corresponds to the Darcy force.

Wall functions. In the case of solving a hydrodynamic problem in the near-wall regions, it is necessary to set the condition of the absence of sliding, or its presence.

No Slip is a boundary condition in the modeling of solid walls. A no-slip wall is a wall where the fluid velocity relative to the wall velocity is zero. For a stationary wall, this means that $\mathbf{u}$=0.

Presence of slip specifies the condition of no penetration, $\mathbf{u}\cdot\mathbf{n}$=0. It is assumed that there are no viscous effects on the sliding wall and, therefore, no wall layer develops. From a modeling perspective, this may be a reasonable approximation if the main effect of the wall is to prevent fluid from escaping the region.

The flow near a solid wall for turbulent flow is different from free flow. The assumptions used in the k-ε model will not be valid near the walls. Although there is a low-Reynolds-number k-ε turbulence model that describes the flow in the near-wall regions, its use is not always practical because of its very high requirements. Therefore, analytical expressions known as near-wall functions are used to describe the flow near the walls. The use of these functions implies a theoretical departure from the physical wall. The wall functions give acceptable predictions as long as they do not exceed some upper bound on the turbulent Reynolds number. This limit is almost never lower than 50, and in many practical problems reaches several hundreds. The highest accuracy is achieved if it is also greater than 25, which roughly corresponds to the beginning of the logarithmic layer. The boundary conditions for the velocity are the condition of no penetration $\mathbf{u}\cdot\mathbf{n}$=0 and the condition of shear stresses. Therefore, we shall solve the problem of hydrodynamic processes assuming the presence of sliding.

Below are the boundary conditions for hydrodynamic flows.

At the boundary G_1:

$$\mathbf{n}^T(-p\mathbf{I}+\mathbf{K})\cdot\mathbf{n}=-p_0; \quad (41)$$

$$\mathbf{u}\cdot\mathbf{t}=0; \quad (42)$$

$$k=\frac{3}{2}(U_{ref}I_T)^2; \quad (43)$$

$$\varepsilon=C_\mu^{3/4}\frac{k^{3/2}}{L_T}, \quad (44)$$

where p_0 is the initial value of pressure at the inlet of the molten metal flow on the surface of the bath, Pa; k and ε are the approximate values of the kinetic energy and energy dissipation rate for the flow of molten metal pouring in [36]; U_{ref} – average flow speed, m/s; I_T is the intensity of turbulence, a dimensionless quantity; L_T=0.07L, where L is the characteristic cross-sectional size of the spot from the flow jet flowing onto the surface of the bath, m.

At the boundaries $G_2...G_6$:

$$\mathbf{u}\cdot\mathbf{n}=0; \quad (45)$$

$$\mathbf{K}-(\mathbf{K}\cdot\mathbf{n})\cdot\mathbf{n}=0; \quad (46)$$

$$\nabla k\cdot\mathbf{n}=0; \quad (47)$$

$$\nabla\varepsilon\cdot\mathbf{n}=0. \quad (48)$$

At the boundary G_7:

$$\mathbf{u}=\mathbf{u}_0; \quad (49)$$

$$\nabla k\cdot\mathbf{n}=0; \quad (50)$$

$$\nabla\varepsilon\cdot\mathbf{n}=0. \quad (51)$$

Here $\mathbf{u}_0$ is the vector of the ingot pulling speed, m/s.

5. 3. Taking into account the processes in the interphase transition zones of metal and its thermophysical characteristics

For the numerical calculation of thermal and hydrodynamic processes in the case of the presence of a phase transition in the metal, the method of finite elements with fixed and movable calculation grids can be applied, if dispersed media are not taken into account.

In the fixed mesh method, the liquid and solid phases are treated as one region. At the same time, the interphase

boundary is not clear and there is a viscous transition zone in it, in which the parameters change according to a certain law relative to the volume fraction of a certain phase. This approach is used to calculate the processes of melting and crystallization of alloys where there is a transition zone between solid and liquid phases.

The moving grid method does not contain an interphase transition zone, so its application is appropriate for processes that occur in pure metals or in metals with a small volume of alloying elements.

With continuous supply of liquid titanium alloy to the crystallizer, the position of the interphase boundary can be calculated using the Phase Field Method [54] with a fixed grid. At the same time, the liquid phase is determined by a temperature higher than the liquidus temperature T_L, the solid phase is determined by a temperature lower than the solidus temperature T_S, and the transition zone is limited by the temperatures T_L and T_S. The volume fraction of metal $F_{L\text{-}S}$ in the transition zone, depending on the temperature, can be described by a smoothed function using the mathematical error function "erf". For the smoothed function:

$$\begin{cases} F_{L-S}(T)=0, T<T_S; \\ F_{L-S}(T)=y_{\text{erf},Down-Up}\left(\begin{matrix}T,x_{\min},x_{\max},y_{\min},\\ y_{\max},x_{\min,\text{erf}},x_{\max,\text{erf}}\end{matrix}\right), T_S\le T\le T_L; \\ F_{L-S}(T)=1, T_L<T, \end{cases} \quad (52)$$

where $y_{\min}=0$, $y_{\max}=1$.

When using the "erf" function, the proposed smoothing function $y_{\text{erf},Down\text{-}Up}$ from the x argument during a step transition along the ordinate axis from the lower (*Down*) level $y_{\min}$ to the higher (*Up*) level $y_{\max}$ will be written in the form:

$$y_{\text{erf},Down-Up}\left(x,x_{\min},x_{\max},y_{\min},y_{\max},x_{\min,\text{erf}},x_{\max,\text{erf}}\right)= =\frac{y_{\max}-y_{\min}}{2}\cdot\left[1+\text{erf}\left(\frac{x-\frac{x_{\min}+x_{\max}}{2}}{\frac{x_{\max}-x_{\min}}{x_{\max,\text{erf}}-x_{\min,\text{erf}}}}\right)\right]+y_{\min}, \quad (53)$$

and its derivative $y'_{\text{erf},Down-Up}$ with respect to the argument x:

$$y'_{\text{erf},Down-Up}\left(x,x_{\min},x_{\max},y_{\min},y_{\max},x_{\min,\text{erf}},x_{\max,\text{erf}}\right)= =\left(y_{\max}-y_{\min}\right)\cdot\frac{1}{\sqrt{\pi}\cdot\frac{x_{\max}-x_{\min}}{x_{\max,\text{erf}}-x_{\min,\text{erf}}}}\times \times\exp\left[-\left(\frac{x-\frac{x_{\min}+x_{\max}}{2}}{\frac{x_{\max}-x_{\min}}{x_{\max,\text{erf}}-x_{\min,\text{erf}}}}\right)^2\right], \quad (54)$$

and the smoothing function $y_{\text{erf},Up\text{-}Down}$ during a step transition along the ordinate axis from a higher level $y_{\max}$ to a lower level $y_{\min}$ takes the following form:

$$y_{\text{erf},Up-Down}\left(x,x_{\min},x_{\max},y_{\min},y_{\max},x_{\min,\text{erf}},x_{\max,\text{erf}}\right)= =\frac{y_{\max}-y_{\min}}{2}\cdot\left[1-\text{erf}\left(\frac{x-\frac{x_{\min}+x_{\max}}{2}}{\frac{x_{\max}-x_{\min}}{x_{\max,\text{erf}}-x_{\min,\text{erf}}}}\right)\right]+y_{\min}, \quad (55)$$

and its derivative $y'_{\text{erf},Up-Down}$ with respect to the argument x:

$$y'_{\text{erf},Up-Down}\left(x,x_{\min},x_{\max},y_{\min},y_{\max},x_{\min,\text{erf}},x_{\max,\text{erf}}\right)= =-\left(y_{\max}-y_{\min}\right)\cdot\frac{1}{\sqrt{\pi}\cdot\frac{x_{\max}-x_{\min}}{x_{\max,\text{erf}}-x_{\min,\text{erf}}}}\times \times\exp\left[-\left(\frac{x-\frac{x_{\min}+x_{\max}}{2}}{\frac{x_{\max}-x_{\min}}{x_{\max,\text{erf}}-x_{\min,\text{erf}}}}\right)^2\right]. \quad (56)$$

Here, $x_{\min}$, $x_{\max}$ are the specified minimum and maximum values along the abscissa axis, at which the minimum and maximum values along the ordinate axis $y_{\min}$, $y_{\max}$ approach their specified values; $x_{\min,\text{erf}}$, $x_{\max,\text{erf}}$ are the minimum and maximum values along the abscissa axis of the "erf" function, at which it approaches the values along the ordinate axis –1 and 1. Usually, at $x_{\min,\text{erf}}=-2$, the function $\text{erf}(-2)=-0.99532$, and at $x_{\max,\text{erf}}=2$, the function $\text{erf}(2)=0.99532$, which is a good approximation to –1 and 1, but if a greater approximation is needed, the value $x_{\min,\text{erf}}=-e$ can be taken, where the function $\text{erf}(-e)=-0.99988$, and when $x_{\max,\text{erf}}=e$, the function $\text{erf}(e)=0.99988$.

The use of the "erf" function is appropriate since it is embedded into almost all computer calculation packages, and, accordingly, it is relatively fast for calculations.

Fig. 2 shows the dependences $y_{\text{erf},Down\text{-}Up}$, $y_{\text{erf},Up\text{-}Down}$ and $y'_{\text{erf},Down\text{-}Up}$, $y'_{\text{erf},Up\text{-}Down}$ on temperature T at $x_{\min}=T_S$; $x_{\max}=T_L$, values $y_{\min}=0$; $y_{\max}=1$ and $x_{\min,\text{erf}}=-2$, $x_{\max,\text{erf}}=2$. Essentially, the $y_{\text{erf},Down\text{-}Up}$ curve reflects the increasing dependence of the $F_{L\text{-}S}$ value, and $y_{\text{erf},Up\text{-}Down}$ – the decreasing dependence of the value $(1-F_{L\text{-}S})$ in the two-phase zone of the liquidus-solidus transition.

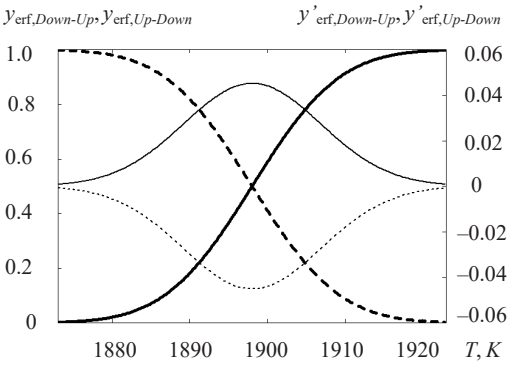

Fig. 2. Dependences on temperature T:
$y_{\text{erf},Down\text{-}Up}$ – continuous thickened growing curve;
$y_{\text{erf},Up\text{-}Down}$ – intermittent thickened falling curve;
$y'_{\text{erf},Down-Up}$ – a continuous thinned curve with positive values;
$y'_{\text{erf},Up-Down}$ – an intermittent thinned curve with negative values

By applying these functions, it is possible to obtain the dependences of the $F_{L\text{-}S}$ and $F_{\alpha-\beta}$ values in the corresponding temperature ranges, using similar formulae (52).

For the considered alloy, the temperatures are: on the artificially extended boundaries of the α–β phase transition $T_\alpha=1253$ K, $T_\beta=1283$ K at the actual temperature $T_{\alpha-\beta}=1283$ K; on the boundaries of the *S*–*L* of the phase transition $T_S=1873$ K, $T_L=1923$ K, with the actual tempera-

ture $T_{L\text{-}S}$=1923; temperature of separation of the ingot from the wall of the crystallizer T_{sep}=1640 K; evaporation temperature T_{ev}=1970 K; metal temperature at the inlet to the crystallizer T_{in}=2061 K. Latent heat (enthalpy) of phase transitions relative to 25 °C (298 K): $H_{\alpha}-H_{25}=6.36\cdot10^5$ J/kg, $H_{\beta}-H_{25}=6.84\cdot10^5$ J/kg and $H_{\alpha-\beta}=H_{\beta}-H_{\alpha}=4.8\cdot10^4$ J/kg; $H_S-H_{25}=1.180\cdot10^6$ J/kg, $H_L-H_{25}=1.466\cdot10^5$ J/kg and $H_{L\text{-}S}=H_L-H_S=2.86\cdot10^5$ J/kg.

It should be noted that the introduction into consideration of the temperature range of phase transitions, in which the thermophysical properties of the material do not have sharp stepwise jumps, but smoothly change in an artificial range set by the user, is a well-known approach [24]. This approach is widely used in the modeling of thermal processes.

A key element of the modeling approach is the introduction of a so-called soft zone at the solid-liquid interface, where thermophysical properties are "smeared" in a user-specified range of melting temperatures.

The accuracy of the mathematical description of the thermophysical characteristics of the titanium alloy as a function of temperature determines the accuracy of the calculations of all parameters and characteristics in the simulation of the movement of the hydrodynamic flows of the titanium alloy in the process of melting the ingot during EBM. Therefore, important attention should be paid to the performance of this task.

It is known that the finite element numerical method is sensitive to gaps in function values and sharp stepwise jumps in values. Stepwise jumps in values are generally observed at α-β and *L-S* phase transitions. If there is a step transition, then the method cannot always find a solution and the calculations fail. It is important to make such a mathematical description of the functions so that there is a smooth transition in stepwise jumps of values. It is convenient to realize this with the obtained functions $y_{\text{erf},Down\text{-}Up}$ and $y_{\text{erf},Up\text{-}Down}$, or using the values $F_{\alpha-\beta}$, $1-F_{\alpha-\beta}$, $F_{L\text{-}S}$, $1-F_{L\text{-}S}$, taking into account the increase or decrease of the values in the phase transitions. The approximate dependences of the thermophysical parameters of the titanium alloy are constructed exactly in this way and have smooth transitions in stepwise jumps of values (Fig. 3).

Fig. 3 shows approximation curves of the simulated characteristics of the Ti-6Al-7Nb alloy used in the calculations versus temperature.

5. 4. Results of mathematical modeling of turbulent hydrodynamic processes and temperature fields in the ingot

A through-flow crystallizer with an internal diameter of 110 mm and a height of 150 mm was used for the research. The ingot extraction speed was chosen to be 20 kg/h (0.489 m/h). The pouring of pre-molten metal from the intermediate container onto the surface of the bath takes place near the wall of the crystallizer in a square spot of 10×10 mm with a speed of the melt jet of 52.4 m/h. The surface of the molten metal is heated by an electron beam with a power of 16 kW with an efficiency of 75 %, which moves in a circle around the periphery of the melt bath with a Gaussian distribution of the thermal power from the electron beam (Fig. 4).

The number of nodes of the calculation grid was taken at the level of $2.7\cdot10^6$.

Calculations were performed for three-dimensional modeling of the system under consideration. The simulation results are shown in Fig. 5–9.

Fig. 5, *a* shows the directions of the velocity vectors of liquid metal flows, with the deduction of the ingot pulling speed downwards in the axial direction. A cross-section along the vertical axis of symmetry of the ingot through the middle of a conditional spot on the surface of the bath from a stream of liquid metal poured into the bath is considered. The size of the vectors is chosen on a logarithmic scale proportional to the speed of the melt movement.

Fig. 5, *b* shows a plot of temperature distribution on the surface of the liquid metal bath under the Gaussian distribution of the heat power floor from the electron beam along the periphery of the melt.

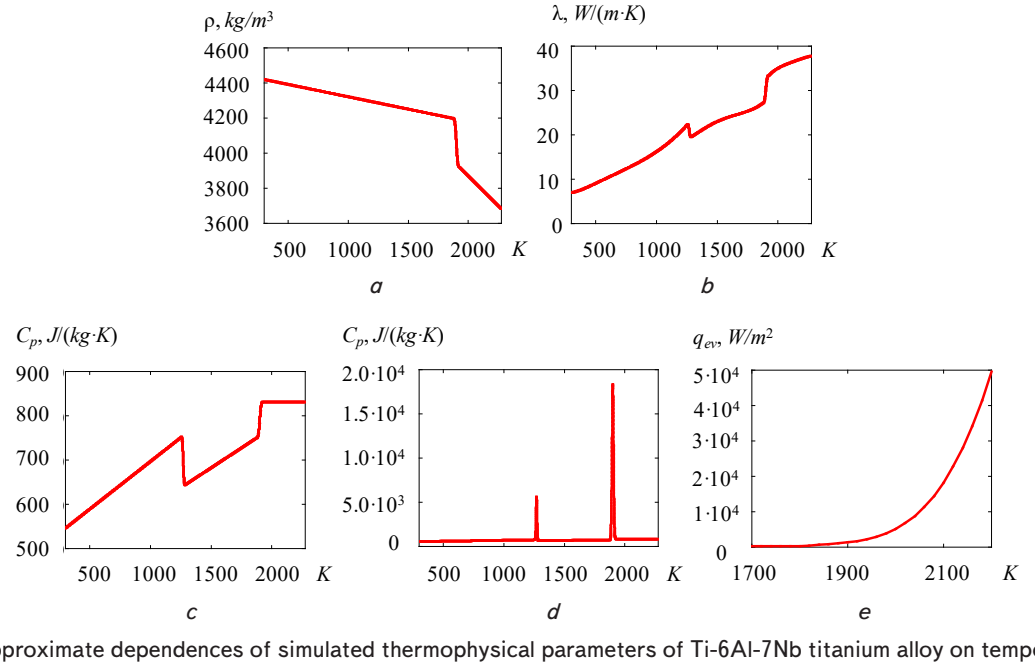

Fig. 3. Approximate dependences of simulated thermophysical parameters of Ti-6Al-7Nb titanium alloy on temperature *T*: *a* – specific density ρ; *b* – thermal conductivity λ; *c* – specific heat capacity C_p; *d* – specific heat capacity C_p taking into account the latent heat of phase transitions α–β and *L-S*; *e* – evaporation losses from the surface of the melt

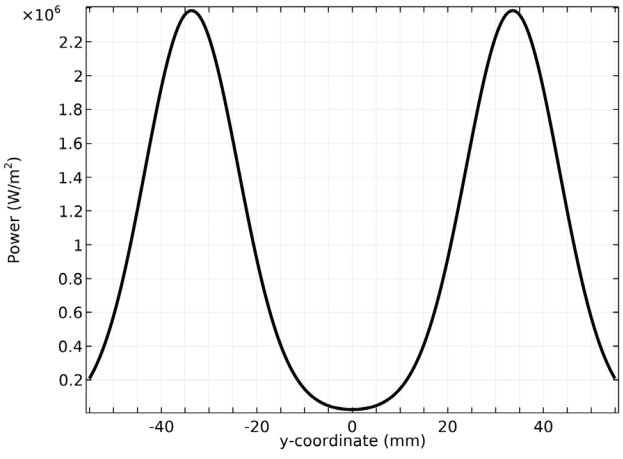

Fig. 4. Distribution of the thermal power of an electron beam over the surface of the ingot

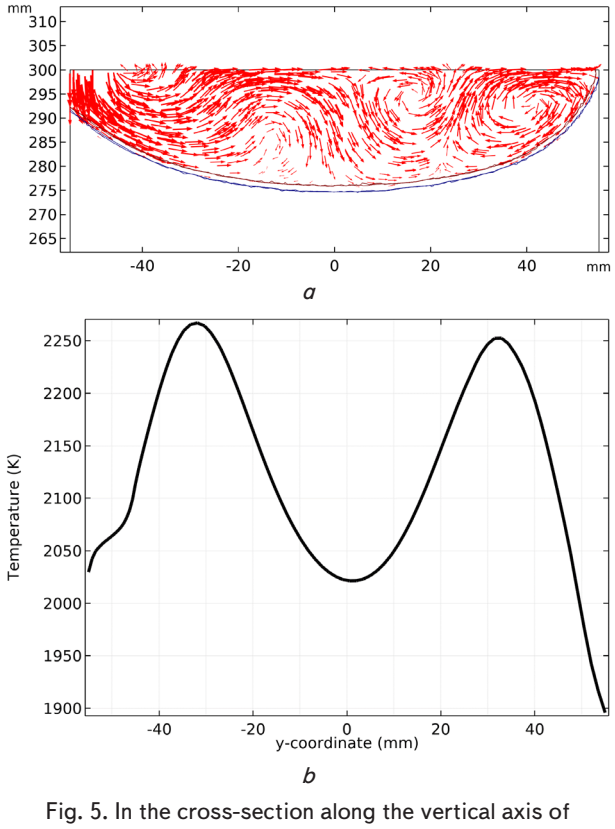

Fig. 5. In the cross-section along the vertical axis of symmetry of the ingot through the middle of the conditional spot on the surface of the bath from the stream of liquid metal pouring into the bath, the following are presented: *a* — flows of liquid metal in the bath; *b* — temperature on the surface of the bath

Fig. 6, *a* demonstrates the directions of the velocity vectors of liquid metal flows, with the deduction of the ingot pulling speed downwards in the axial direction. A cross-section along the vertical axis of symmetry of the ingot at an angle of 90° from the middle of the conventional spot on the surface of the bath from the jet of liquid metal poured into the bath is considered. This is a plane perpendicular to the plane from Fig. 5, *a*. 1/2 part of the drawing is presented since its other half is symmetrical.

Fig. 6, *b* shows a plot of temperature distribution on the surface of the bath of molten metal.

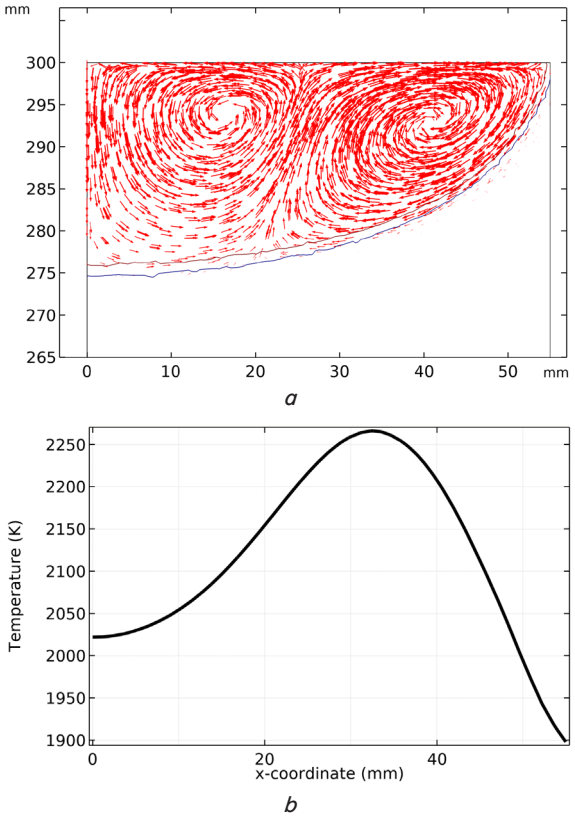

Fig. 6. In the cross-section along the vertical axis of symmetry of the ingot at an angle of 90°, the following are presented: *a* — streams of liquid metal in the bath; *b* — temperature on the surface of the bath

Fig. 7 demonstrates the three-dimensional distribution of the temperature field and the direction of the velocity vectors of the metal flows in the crystallizer with the deduction of the ingot pulling speed to the bottom.

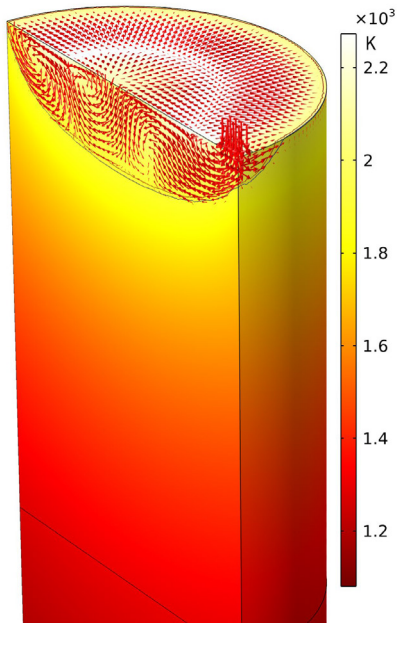

Fig. 7. Three-dimensional distribution of the temperature field and metal flows in the crystallizer with deduction of the ingot pulling speed to the bottom

Fig. 8 shows the distribution of the temperature field and metal flows in the crystallizer (top view).

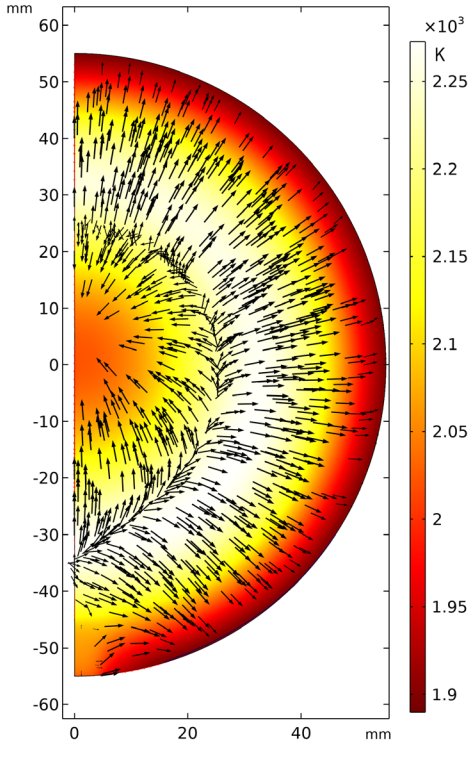

Fig. 8. Distribution of the temperature field and metal flows in the crystallizer (top view)

Fig. 9 demonstrates the directions of liquid metal flows, taking into account the speed of drawing the ingot to the bottom in the axial direction. A cross-section along its vertical axis of symmetry through the middle of a conditional spot on the surface of the bath from a jet of liquid metal pouring into the bath is considered.

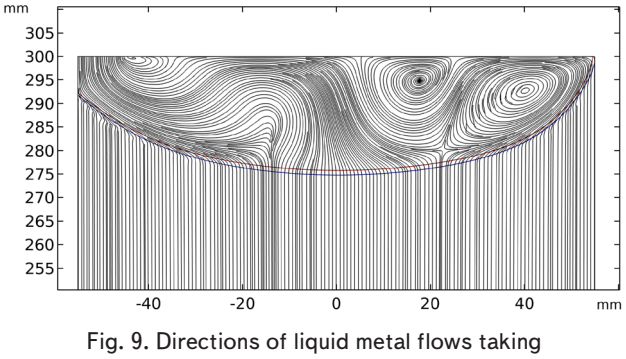

Fig. 9. Directions of liquid metal flows taking into account the rate of pulling the ingot downwards in the axial direction in a cross-section along its vertical axis of symmetry

For experimental verification of the constructed mathematical model according to the technological parameters used in the simulation, namely: melting rate, 20 kg/h; power of electron beam heating of the surface of the melt in the crystallizer, 16 kW. Using the EBM technique with an intermediate capacity [55, 56], a Ti-6Al-7Nb titanium alloy ingot with a diameter of 110 mm and a length of 630 mm was obtained (Fig. 10), from which a transverse template was cut (Fig. 11).

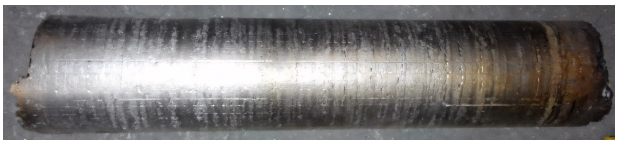

Fig. 10. An ingot of Ti-6Al-7Nb titanium alloy with a diameter of 110 mm and a length of 630 mm, obtained by the technique of electron beam melting [57]

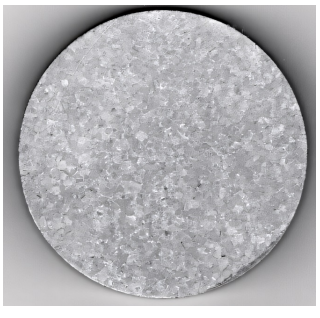

Fig. 11. Macrostructure of the cast metal of a Ti-6Al-7Nb titanium alloy ingot with a diameter of 110 mm [57]

Fig. 11 shows the macrostructure of the metal of the transverse template of the Ti-6Al-7Nb titanium alloy ingot with a diameter of 110 mm, melted by the EBM technique. The structure of the metal was revealed by the method of chemical etching of the surface of the template.

6. Discussion of results of the mathematical modeling of turbulent processes of heat and mass transfer

Taking as a basis the most successful elements of the implementation of mathematical models, mainly from [22, 23], by eliminating the main unresolved issues noted in them, we modernized them to solve the problem of finding the necessary parameters for the formation of a high-quality ingot of the latest medical titanium alloy Ti-6Al-7Nb. Faster pouring of liquid metal into a crystallizer of smaller diameter is taken into account, which led to the formation of turbulent flows of liquid metal. Heating of the melt surface in the crystallizer by only one electron gun is taken into account. The approach to constructing approximate dependences of thermophysical parameters of metal on temperature has been modernized, in which sharp jumps and breaks in the values of these functions in two-phase zones have been eliminated at the points of phase transitions. Another function has been proposed to take into account the heat capacity of the phase transition. The parameters of heat dissipation into the wall of the crystallizer from the liquid metal of the bath and the parameters of heat radiation from the ingot surfaces were more precisely determined. That has made it possible to identify the regularities of turbulent heat and mass transfer processes during the formation of an ingot of the newest titanium alloy Ti-6Al-7Nb with sufficient accuracy for practice.

Owing to the constructed mathematical model of thermal (basic formulae (1), (2), additional formulae (3) to (8), (11) to (13), and boundary conditions formulae (14) to (32)) and turbulent hydrodynamic (basic formulae (33) to (35), k-ε formulae of the model (36) to (40) and boundary conditions formulae (41) to (51)) of processes in the ingot, as a result of three-dimensional mathematical modeling, we have

calculated temperature fields and hydrodynamic flows in the case of forming an ingot of the newest titanium alloy Ti-6Al-7Nb by the EBM technique. At the same time, thermophysical characteristics of the metal, which depend on temperature, were applied, and interphase transition zones were taken into account. That has made it possible to reveal the regularities of the distribution of hydrodynamic flows in the liquid metal and temperature fields, as well as the crystallization front of the metal during the formation of the ingot.

A characteristic feature of the modeling was that thermal and hydrodynamic processes during ingot formation by the EBM technique were investigated for the newest titanium alloy Ti-6Al-7Nb. Smelting of ingots took place in a continuous crystallizer with an internal diameter of 110 mm. Castings are intended for the needs of the medical industry.

Fig. 5, *a* demonstrates that the streams of molten metal spread from the place of its pouring, forming several vortices, in contrast to one large vortex at 5.5 times larger diameter of the crystallizer – 600 mm from work [22]. The lack of axial symmetry of the melt movement is due to the ingress of the liquid metal current along the wall of the crystallizer through a spot measuring 10x10 mm and confirms the need to use three-dimensional modeling. Fig. 5, *a* shows the temperature isotherms of the liquidus T_L (upper curve) and solidus T_S (lower curve) at the boundary of the crystallization front. The position and geometry of this front (Fig. 5, 6, 9) largely determines the quality of ingot formation and the concentration of distribution of alloying elements in its volume. The flatter the front, the more uniform the distribution of alloying elements in the radial direction of the ingot and the more uniform the structure of the solid metal. In comparison with the crystallizer of a larger diameter from work [22], this condition is ensured to a greater extent for a crystallizer with a diameter of 110 mm.

An important criterion for the quality of ingots of titanium alloys is the smooth appearance of their surface. Therefore, during melting, it is also necessary to strive for the liquid metal of the bath to be in contact with the wall of the crystallizer as little as possible, in order to avoid corrugations on the side surfaces of the ingots. The correct choice of the position of the electron beam in the radial direction on the surface of the bath provides this condition, and the intensity of the beam – the depth and geometry of the crystallization front. From the plot of temperature distribution on the surface of the bath of molten metal (Fig. 5, *b*), one can see that the maxima on the curve are due to the concentrations of thermal power introduced by the beam of the electron gun. It is this distribution of temperatures that contributes to ensuring the required shape of the metal crystallization front in Fig. 5, *a*.

In the cross-section of the ingot in Fig. 6, *a*, two developed eddy currents and two more symmetrical to them are observed.

Flows of molten metal for different vertical sections of the ingot in Fig. 5, 6, *a* differ because they depend on the place where the liquid metal is poured into the crystallizer.

This is well illustrated by the three-dimensional distribution of the temperature field and metal flows in the crystallizer in Fig. 7, 8. The top view shows a pronounced radial distribution of metal flows, largely caused by the concentration of thermal power from the electron beam and the action of flows from liquid metal pouring into the crystallizer.

Fig. 9 illustrates a complete picture of the distribution of the speed of hydrodynamic flows in the ingot, taking into account the speed of pulling the ingot downwards in the axial direction.

The results of the calculations of the trajectories of metal movement showed the adequate use of the Darcy function to inhibit the movement of metal in the solid phase.

As a result of the calculations, it was found that the heat transfer in the liquid phase of the ingot in the turbulent regime is mainly caused by the heat and mass exchange due to the movement of the molten metal. At the same time, the power of the electron beam and the type of its flooring on the surface of the bath have a very significant effect on heat and mass exchange.

In the 110 mm diameter Ti-6Al-7Nb titanium alloy cast by the EBM technique (Fig. 10), the surface is free of casting defects, there are practically no corrugations on it, and there is only some roughness. Such ingots at the current level of development of the melting of titanium alloys are defined as ingots of high quality. The technology of casting such ingots from the Ti-6Al-7Nb titanium alloy, the main parameters of melting, and the analysis of the structure of the obtained metal were described in detail in [57]. From the macrostructure of the metal of the transverse template cut from this ingot (Fig. 11), one can see that the structure of the metal is homogeneous over the entire cross-sectional area of the ingot, which confirms its high quality. This indirectly confirms the presence of a crystallization front close to flat.

Casts are intended for the needs of the medical industry for the manufacture of light and ultra-strong endoprostheses and implants, which are chemically neutral and biologically and biomechanically compatible with the human body and do not cause rejection.

Among the factors that affected the accuracy of the calculations are the simplifications and assumptions used during the construction of the mathematical model, the number of which can be reduced in the further improvement of the model. But they did not fundamentally affect the revealed general tendencies of ingot formation.

Our work is useful for foundry engineers in order not to rely on the extremely expensive experimental method of trial melting in the search for the necessary parameters of the melting regimes. This refers to the determination of the parameters of technological modes, when it is necessary to apply a crystallizer with different dimensions, different from the one for which the melting modes have already been worked out, or to use a new alloy. Therefore, with the help of mathematical modeling, it is possible to calculate and predict the necessary operating parameters of melting, which significantly reduces the cost and simplifies the stage of searching for parameters of melting modes.

Since the improved and refined approximation dependences of the thermophysical parameters of the titanium alloy Ti-6Al-7Nb are used in the work, the modeling of heat and mass transfer processes for this alloy has high reliability, close to practical results. If one switches to another titanium alloy, it is necessary to determine and approximate the dependence of its thermophysical parameters on temperature. Therefore, the use of a mathematical model with thermophysical parameters of the Ti-6Al-7Nb alloy for other alloys could lead to the possible obtaining of insufficiently reliable calculation data.

It should be noted that at a reduced rate of liquid metal supply to the crystallizer, the turbulent hydrodynamic process of the molten metal flows in the bath can go into the laminar mode of flow spreading. The same applies to ingots of large diameter. In this case, the mathematical model of turbulent heat-mass exchange processes would give notoriously unreliable patterns of the distribution of the temperature field and hydrodynamic flows of the liquid metal, and accordingly,

the shape of the metal crystallization profile. This is a drawback of the developed model. Therefore, in order to study the laminar processes of the movement of melt flows in the Ti-6Al-7Nb titanium alloy ingot, it is necessary to build an appropriate mathematical model. In the future, this will be an advancement of research into this area.

7. Conclusions

1. A three-dimensional mathematical model of thermal processes in the ingot, which is melted by the electron beam melting technique, in which the beam moves in a circle around the periphery of the melt bath according to the Gaussian distribution of the thermal power from the beam, has been built. The model, subject to certain defined limitations, makes it possible to calculate the stationary temperature field in the case of turbulent movement of the molten metal with consideration of the coefficient of turbulent thermal conductivity, coefficient of turbulent dynamic viscosity, turbulent Prandtl number, and viscous dissipation. The process of heat transfer is used, taking into account the near-wall functions and radiation.

2. A three-dimensional mathematical model of stationary turbulent hydrodynamic processes in the melt of a cylindrical ingot was constructed, based on the Reynolds-averaged Navier-Stokes equations (RANS). For the closure of these equations, the classical semi-empirical k-ε turbulence model was used, which allowed us to calculate the hydrodynamic flows of molten metal in the bath with melt.

3. To provide a correct solution to the problem of calculating the turbulent processes of heat and mass transfer in the ingot, functional dependences of the thermophysical characteristics of the newest titanium alloy Ti-6Al-7Nb on temperature were modeled. The mathematical error function "erf" was used for the interphase zones. This ensured the continuity of the functions and their derivatives for stepwise changes in the values of thermophysical characteristics in phase transitions. The use of the developed dependences of thermophysical parameters on temperature has made it possible to more correctly calculate the specified processes, in relation to the use of averaged values of thermophysical parameters in many mathematical models.

4. Based on the results of mathematical modeling, temperature fields and turbulent hydrodynamic flows of molten metal in a titanium alloy Ti-6Al-7Nb ingot with a diameter of 110 mm were obtained. The geometry of the liquidus-solidus two-phase zone was defined, which determines the crystallization front of the metal, the position and geometry of which significantly affects the quality of the ingot formation. On the basis of calculated data, it was found that the heat transfer in the liquid phase of the ingot under a turbulent mode is mainly due to the heat and mass transfer due to the movement of the molten metal, and the distribution of power of the electron beam on the surface of the bath has a very significant effect on the heat and mass transfer. It is shown that in the case of an electron beam heating power of 16 kW and a melting speed of 20 kg/h, a sufficiently flat crystallization front is formed, which ensures a uniform distribution of alloying elements in the ingot and its homogeneous fine-grained structure.

Conflicts of interest

The authors declare that they have no conflicts of interest in relation to the current study, including financial, personal, authorship, or any other, that could affect the study, as well as the results reported in this paper.

Funding

The research was carried out within the budget-funded scientific work 30.57.21/37 "Development of technologies for obtaining the newest titanium alloys by electron beam melting and articles from them by rolling and 3D printing for the needs of defense and medicine" (2023–2024), State registration number 0123U100870 (06.02.2023), executed according to the resolution of the Presidium of the National Academy of Sciences of Ukraine, dated 13.12.2023, No. 443.

Data availability

All data are available, either in numerical or graphical form, in the main text of the manuscript.

Use of artificial intelligence

The authors confirm that they did not use artificial intelligence technologies when creating the current work.

Acknowledgments

The authors express their sincere gratitude to colleagues from the Institute of Electrodynamics at the National Academy of Sciences of Ukraine, Doctor of Technical Sciences Yuri Horyslavets, PhD Oleksandr Hlukhenky, PhD Oleksiy Bondar, for using the materials of related publications as a background in the construction of a mathematical model [22, 23].

References

1. Tamayo, J. A., Riascos, M., Vargas, C. A., Baena, L. M. (2021). Additive manufacturing of Ti6Al4V alloy via electron beam melting for the development of implants for the biomedical industry. Heliyon, 7 (5), e06892. https://doi.org/10.1016/j.heliyon.2021.e06892
2. Mahlobo, M. G. R., Chikosha, L., Olubambi, P. A. (2022). Study of the corrosion properties of powder rolled Ti–6Al–4V alloy applied in the biomedical implants. Journal of Materials Research and Technology, 18, 3631–3639. https://doi.org/10.1016/j.jmrt.2022.04.004
3. Fellah, M., Labaïz, M., Assala, O., Dekhil, L., Taleb, A., Rezag, H., Iost, A. (2014). Tribological behavior of Ti-6Al-4V and Ti-6Al-7Nb Alloys for Total Hip Prosthesis. Advances in Tribology, 2014, 1–13. https://doi.org/10.1155/2014/451387
4. Bartha, K., Zháňal, P., Stráský, J., Čížek, J., Dopita, M., Lukáč, F., Harcuba, P. et al. (2019). Lattice defects in severely deformed biomedical Ti-6Al-7Nb alloy and thermal stability of its ultra-fine grained microstructure. Journal of Alloys and Compounds, 788, 881–890. https://doi.org/10.1016/j.jallcom.2019.02.173

5. Bolzoni, L., Ruiz-Navas, E. M., Gordo, E. (2017). Evaluation of the mechanical properties of powder metallurgy Ti-6Al-7Nb alloy. Journal of the Mechanical Behavior of Biomedical Materials, 67, 110–116. https://doi.org/10.1016/j.jmbbm.2016.12.005
6. Sun, Y., Huang, B., Puleo, D. A., Schoop, J., Jawahir, I. S. (2016). Improved Surface Integrity from Cryogenic Machining of Ti-6Al-7Nb Alloy for Biomedical Applications. Procedia CIRP, 45, 63–66. https://doi.org/10.1016/j.procir.2016.02.362
7. Wei, G., Tan, M., Attarilar, S., Li, J., Uglov, V. V., Wang, B. et al. (2023). An overview of surface modification, A way toward fabrication of nascent biomedical Ti-6Al-4V alloys. Journal of Materials Research and Technology, 24, 5896–5921. https://doi.org/10.1016/j.jmrt.2023.04.046
8. Oktikawati, A., Riastuti, R., Damisih, D., Nyoman Jujur, I., Paul Setiawan Kaban, A. (2024). Electrochemical characteristic and microstructure of Ti-6Al-7Nb alloy by centrifugal casting for orthopedic implant based on ageing time variations. Eastern-European Journal of Enterprise Technologies, 2 (12 (128)), 6–15. https://doi.org/10.15587/1729-4061.2024.302614
9. Hussain, S. A., Panchal, M., Allamraju, K. V., Rajak, U., Verma, T. N., Brindhadevi, K. (2023). Optimization of wear behavior of heat-treated Ti-6Al-7Nb biomedical alloy by response surface methodology. Environmental Research, 231, 116193. https://doi.org/10.1016/j.envres.2023.116193
10. Biswal, S., Tripathy, S., Tripathy, D. K. (2024). Optimisation of PMEDM process parameters for Ti-6Al-7Nb biomedical material. Materials Today: Proceedings. https://doi.org/10.1016/j.matpr.2024.02.044
11. Cabrini, M., Carrozza, A., Lorenzi, S., Pastore, T., Testa, C., Manfredi, D. et al. (2022). Influence of surface finishing and heat treatments on the corrosion resistance of LPBF-produced Ti-6Al-4V alloy for biomedical applications. Journal of Materials Processing Technology, 308, 117730. https://doi.org/10.1016/j.jmatprotec.2022.117730
12. Xu, X., Li, J., Dong, Z., Zeng, L., Xu, Z., Li, J. (2022). Multiphase modelling of the continuous metallurgical purification process for impurity removing of recycled aluminum. Journal of Materials Research and Technology, 18, 830–840. https://doi.org/10.1016/j.jmrt.2022.03.003
13. Hatič, V., Mavrič, B., Šarler, B. (2020). Simulation of macrosegregation in direct-chill casting – A model based on meshless diffuse approximate method. Engineering Analysis with Boundary Elements, 113, 191–203. https://doi.org/10.1016/j.enganabound.2019.12.006
14. Luo, Y., Zhang, Z. (2019). Numerical modeling of annular electromagnetic stirring with intercooling in direct chill casting of 7005 aluminum alloy billet. Progress in Natural Science: Materials International, 29 (1), 81–87. https://doi.org/10.1016/j.pnsc.2019.01.007
15. Begum, L. (2013). 3-D Transport Phenomena in Vertical Direct. Chill Casting Processes. Montreal, 279.
16. Ufodike, C. O., Nzebuka, G. C., Egole, C. P. (2023). Prediction of Limiting Casting Speed in a Horizontal Direct-Chill Casting through Numerical Modeling and Simulation. Metals, 13 (6), 1071. https://doi.org/10.3390/met13061071
17. Pardeshi, R. (2016). Computational model for multi alloy casting of aluminum rolling ingots. Journal of Manufacturing Processes, 21, 23–29. https://doi.org/10.1016/j.jmapro.2015.10.006
18. Ludwig, A., Rodrigues, C. M. G., Zhang, Z., Zhang, H., Karimi-Sibaki, E., Barati, H. et al. (2021). Important Key Process Simulations in the Field of Steel Metallurgy. BHM Berg- Und Hüttenmännische Monatshefte, 167 (1), 2–9. https://doi.org/10.1007/s00501-021-01184-1
19. Haag, J., Martens, J., Dussoubs, B., Jardy, A., Bellot, J.-P. (2020). Analysis of the Thermal Transfers in a VASM Crucible: Electron Beam Melting Experiment and Numerical Simulation. Metals, 10 (9), 1152. https://doi.org/10.3390/met10091152
20. El Idi, M. M., Karkri, M. (2020). Melting and solidification behavior of PCM embedded in metal foam. COMSOL Conference 2020 Europe. Available at: https://hal.science/hal-02966782
21. Moench, S., Dittrich, R. (2022). Influence of Natural Convection and Volume Change on Numerical Simulation of Phase Change Materials for Latent Heat Storage. Energies, 15 (8), 2746. https://doi.org/10.3390/en15082746
22. Akhonin, S. V., Gorislavets, Yu. M., Glukhenkiy, A. I., Berezos, V. A., Bondar, A. I., Pikulin, A. N. (2019). Modeling Hydrodynamic And Thermal Processes In The Mould In Cold-hearth Electron Beam Melting. Sovremennaâ Èlektrometallurgiâ, 2019 (4), 9–17. https://doi.org/10.15407/sem2019.04.02
23. Akhonin, S. V., Berezos, V. O., Bondar, O. I., Glukhenkii, O. I., Goryslavets, Yu. M., Severin, A. Yu. (2021). Mathematical modeling of hydrodynamic and thermal processes at crystallization of titanium ingots produced by EBM. Sovremennaâ Èlektrometallurgiâ, 2021 (1), 27–34. https://doi.org/10.37434/sem2021.01.03
24. Rubinetti, D., Weiss, D. A., Chaudhuri, A., Kraniotis, D. (2018). Modeling Approach to Facilitate Thermal Energy Management with Phase Change Materials (PCM). COMSOL Conference. Available at: https://www.comsol.com/paper/modeling-approach-to-facilitate-thermal-energy-management-with-phase-change-mate-63481
25. Heat Transfer Module User's Guide. Available at: https://doc.comsol.com/5.4/doc/com.comsol.help.heat/HeatTransferModuleUsersGuide.pdf
26. Panton, R. L. (2013). Incompressible Flow. John Wiley & Sons. https://doi.org/10.1002/9781118713075
27. Civan, F., Sliepcevich, C. M. (1987). Limitation in the Apparent Heat Capacity Formulation for Heat Transfer With Phase Change. Available at: https://citeseerx.ist.psu.edu/document?repid=rep1&type=pdf&doi=a164ded6feb6d03531c1b0b43b8ab8f45b0cf747
28. Zhu, Z., Zhou, R., Li, X., Xiong, W., Li, Z. (2022). Flow Field and Inclusions Movement in the Cold Hearth for the Ti-0.3Mo-0.8Ni Alloy. Crystals, 12 (10), 1471. https://doi.org/10.3390/cryst12101471
29. Lacasse, D., Turgeon, É., Pelletier, D. (2004). On the judicious use of the *k*-ε model, wall functions and adaptivity. International Journal of Thermal Sciences, 43(10), 925–938. https://doi.org/10.1016/j.ijthermalsci.2004.03.004

30. Weigand, B., Ferguson, J. R., Crawford, M. E. (1997). An extended Kays and Crawford turbulent Prandtl number model. International Journal of Heat and Mass Transfer, 40 (17), 4191–4196. https://doi.org/10.1016/s0017-9310(97)00084-7
31. Kays W. M., Crawford M. E. (1993). Convective Heat and Mass Transfer. McGraw-Hill Science/Engineering/Math, 480.
32. Kays, W., Crawford, M., Weigand, B. (2005). Convective Heat and Mass Transfer. McGraw-Hill.
33. Jischa, M., Rieke, H. B. (1979). About the prediction of turbulent prandtl and schmidt numbers from modeled transport equations. International Journal of Heat and Mass Transfer, 22 (11), 1547–1555. https://doi.org/10.1016/0017-9310(79)90134-0
34. Fuchs, H. (1973). Wärmeübergang an strömendes Natrium. Würenlingen, 257.
35. Launder, B. E., Spalding, D. B. (1974). The numerical computation of turbulent flows. Computer Methods in Applied Mechanics and Engineering, 3 (2), 269–289. https://doi.org/10.1016/0045-7825(74)90029-2
36. Versteeg, H. K., Malalasekera, W. (2007). An Introduction to Computational Fluid Dynamics: The Finite Volume Method. Pearson Education.
37. Arpaci, V., Larsen, P. (1984). Convection Heat Transfer. Prentice Hall, 512.
38. Bushok, H. F., Venher, Ye. F. (2002). Fizychni osnovy mekhaniky. Molekuliarna fizyka i termodynamika. Knyha 1. Kyiv: Vyshcha shkola, 375.
39. Truong, V.-D., Hyun, Y.-T., Won, J. W., Lee, W., Yoon, J. (2022). Numerical Simulation of the Effects of Scanning Strategies on the Aluminum Evaporation of Titanium Alloy in the Electron Beam Cold Hearth Melting Process. Materials, 15 (3), 820. https://doi.org/10.3390/ma15030820
40. Nogovicyn, A. V., Podol'cev, A. D., Kucheryavaya, I. N. (2015). Chislennoe modelirovanie gidrodinamicheskih i teplovyh processov pri nepreryvnoj dvuhvalkovoj razlivke stali. Metall i lit'e Ukrainy, 3 (262), 15–20.
41. Nogovicyn, A. V., Podol'cev, A. D., Kucheryavaya, I. N. (2016). Turbulentnyj gidrodinamicheskij i teplovoj processy pri dvuhvalkovoj razlivke stali (trekhmernoe komp'yuternoe modelirovanie). Processy lit'ya, 2 (116), 23–34.
42. Yao, L., Maijer, D. M., Cockcroft, S. L., Fiore, D., Tripp, D. W. (2018). Quantification of heat transfer phenomena within the melt pool during the plasma arc re-melting of titanium alloys. International Journal of Heat and Mass Transfer, 126, 1123–1133. https://doi.org/10.1016/j.ijheatmasstransfer.2018.06.051
43. Belyaev, N. M. (1989). Osnovy teploperedachi. Kyiv, 343.
44. Wilcox, D. C. (2006). Turbulence modeling for CFD. California: DCW Industries Inc., 515.
45. Pope, S. B. (2000). Turbulent Flow. Cambridge University Press, 771.
46. Launder, B. E., Sharma, B. I. (1974). Application of the energy-dissipation model of turbulence to the calculation of flow near a spinning disc. Letters in Heat and Mass Transfer, 1(2), 131–137. https://doi.org/10.1016/0094-4548(74)90150-7
47. Jones, W. P., Launder, B. E. (1972). The prediction of laminarization with a two-equation model of turbulence. International Journal of Heat and Mass Transfer, 15(2), 301–314. https://doi.org/10.1016/0017-9310(72)90076-2
48. Launder, B. E., Spalding, D. B. (1972). Mathematical Models of Turbulence. New York: Academic Press, 169.
49. Baraniuk, O. V., Vorobiov, M. V., Rachynskyi, A. Yu. (2023). CFD-modeliuvannia protsesiv teploobminu i hidrodynamiky zasobamy prohramnoho kompleksu. Kyiv: Politekhnika, 164.
50. Larsson, J. (1998). Numerical Simulation of Turbulent Flows for Turbine Blade Heat Transfer Applications. Gothenburg: Chalmers University of Technology, 57.
51. Avnaim, M. H., Levy, A., Mikhailovich, B., Ben-David, O., Azulay, A. (2016). Comparison of Three-Dimensional Multidomain and Single-Domain Models for the Horizontal Solidification Problem. Journal of Heat Transfer, 138 (11). https://doi.org/10.1115/1.4033700
52. Ben-David, O., Levy, A., Mikhailovich, B., Azulay, A. (2013). 3D numerical and experimental study of gallium melting in a rectangular container. International Journal of Heat and Mass Transfer, 67, 260–271. https://doi.org/10.1016/j.ijheatmasstransfer.2013.07.058
53. Mizukami, H., Funagane, H., Kitaura, T., Takeda, Y., Wada, M., Shirai, Y., Umeda, S. (2022). Removal Technology of Inclusion from Titanium Alloy Melt in Hearth. Nippon Steel Technical Report.
54. Boettinger, W. J., Warren, J. A., Beckermann, C., Karma, A. (2002). Phase-Field Simulation of Solidification. Annual Review of Materials Research, 32 (1), 163–194. https://doi.org/10.1146/annurev.matsci.32.101901.155803
55. Akhonin, S., Pikulin, O., Berezos, V., Severyn, A., Erokhin, O., Kryzhanovskyi, V. (2022). Determining the structure and properties of heat-resistant titanium alloys VT3-1 and VT9 obtained by electron-beam melting. Eastern-European Journal of Enterprise Technologies, 5 (12 (119)), 6–12. https://doi.org/10.15587/1729-4061.2022.265014
56. Akhonin, S. V., Pikulin, O. M. (2019). Investigation of Effect of Electron Beam Surface Treatment of Titanium Alloy Ingots on Structure and Properties of Melted Metal. IOP Conference Series: Materials Science and Engineering, 582 (1), 012047. https://doi.org/10.1088/1757-899x/582/1/012047
57. Berezos, V. O., Akhonin, D. S. (2023). Electron beam melting of titanium alloys for medical purposes. The Paton Welding Journal, 2023 (6), 41–48. https://doi.org/10.37434/tpwj2023.06.06